RSC Advances

ROYAL SOCIETY OF CHEMISTRY

www.rsc.org/advances

Pseudo-first order reaction kinetics and thermodynamic properties study of neem oil esterification using MgO grafted natural hydroxyapatite

Himadri Sahu, Kaustubha Mohanty*

Department of Chemical Engineering, Indian Institute of Technology Guwahati, Guwahati – 781039, India

Abstract

In this work, waste fish bone was used as a source of natural hydroxyapatite which was later used for the preparation of metal grafted catalyst. Calcium phosphate is the main component of fish bone which has relatively high catalytic activity, good thermal and chemical stability, and can be used for various applications. Magnesium oxide (MgO) was used for grafting due to its high specific surface area. It can be used as active phase during catalysis which influences the selectivity and activity of catalytic reactions. In the present investigation, the waste fish bone-derived catalysts were characterized in detail and used for the esterification of neem oil (*Azadirachta indica*). The highest methyl ester yield of 96.7% was obtained at 1:15 oil to methanol ratio, 70°C reaction temperature and 6 wt.% catalyst loading. The catalytic effect on yield and reusability of the catalyst was also studied. Subsequently, a kinetic model was developed and the thermodynamics properties of the process are illustrated. Overall the whole work gives a new direction towards the development of heterogeneous catalyst from bio wastages.

Key words: waste fish bone, esterification, reaction kinetics, neem oil

*Corresponding author. Email: kmohanty@iitg.ernet.in (K. Mohanty)

Tel.: 91-361-2582267; Fax: 91-361-2582291

1. Introduction

Globally in excess of ninety-one million tons of fish are caught annually and around 55% of this are used for human consumption, while the rest are discarded.[1] Most of the fish used for human consumption are deboned and exported. The bones are usually discarded without any further use and thus create undesirable impact on the environment. These bones are rich source of calcium phosphate, popularly also known as Hydroxyapatite (HAp), with a stoichiometric formula $Ca_{10}(PO_4)_6(OH_2)$. It is therefore advisable to use this low-cost source of HAp for some meaningful purpose which will address the waste management problem also.

There are few differences between synthetic and natural hydroxyapatite. Natural HAp has better dynamic response to the environment, high catalytic activity and good thermo-chemical stability than the synthetic HAp.[2, 3] As far as solubility and activity is concerned, crystallographic structure plays an important role. In line to synthetic HAp, the natural HAp has perturbed nanostructures and nonstoichiometric composition with low hydroxyl content. As physical and chemical properties depend on structure, natural HAp will lead to good results.[4] Because of these properties HAp can be used as a heterogeneous catalyst. Although natural HAp has favorable structure but the BET surface area is bit low, which can be increased by grafting metal ions on to it. Venkatesan et al. developed nano-hydroxyapatite from salmon fishbone and was characterized using various techniques. From the analysis it is clearly shown that it has potential to give a metal support on it. The SAED pattern showed the crystalline nature of the material.[5] Sasaki and Goto also extracted hydroxyapatite from four types of fish bone and compared with commercial grade hydroxyapatite. They showed ion-exchange efficiency, but however application in reaction field was missing.[6] Chakraborty and RoyChowdhury tried to dope Cu^{2+} on hydroxyapatite derived from waste fishbone and the heterogeneous catalyst was used for esterification of oleic

acid. However, the catalyst has very low surface area, pore volume as well as very poor thermal stability. In the literature it was mentioned that there are uniform pores but the SEM image shows flat surface at 5 μm range which is contradictory. Although above 90% conversion of oleic acid was shown but the effect on mixture of fatty acid i.e. vegetable oil was not discussed.[7] Considering all these aspects, the objective of the present work is decided.

In the present work, Natural HAp collected from waste fish bone was used as a base material for metal grafting to carry out esterification of neem (*Azadirachta indica*) oil. From literature, it was found that MgO alone was proved to be a very good catalyst in esterification reaction.[8-11] Therefore Mg metal ion was grafted on to the natural HAp by wet impregnation method followed by calcination to increase the surface area of HAp as well as it's catalytic activity. In this grafted catalyst both the HAp and MgO will act as an active source for the adsorption of reactants during the reaction.

2. Materials and Detailed Methodology

2.1 Materials

From IIT Guwahati hostel messes cooked waste fish bone was collected. Few chemicals *viz.* 25% aqueous ammonia solution, methanol and Magnesium Sulfate ($MgSO_4.7H_2O$) were procured from Sigma Aldrich, India and were used as it is without any further treatment.

2.2 Preparation methodology

Fish bone was washed properly to remove proteinaceous part and sun dried for 2 days. After that oily matters was removed completely by dipping in acetone for 24 h and dried at 60 °C. The fishbone was crushed and natural hydroxyapatite (N_{HAp}) was obtained. Magnesium sulfate was used as the precursor for metal ions during wet impregnation.[12] Following the

method, 1:1 wt. proportions of N_{HAp} and MgO were prepared. 30 g of $MgSO_4.7H_2O$ was added to 100 mL of water to get a solution of Magnesium sulfate. To this solution, 30 g of fine powder of N_{HAp} was added gradually and blended rigorously using a mechanical agitator under aggregate reflux time of 30 min. 25% aqueous ammonia solution was used to maintain pH at 11. The entire solution was mechanically stirred for 2 h at 700 rpm at 60 °C. The final solution was kept for 24 h at room temperature so as to allow the deposition of Magnesium ions on N_{HAp}. After that mother liquor was vacuum filtered and the sticky precipitate obtained was dried in hot air oven. The dried mass was then calcined at 650 °C for 3 h and final Mg grafted N_{HAp} (Mg-N_{HAp}) was sent for characterization.

2.3 Catalyst, raw neem oil (RNO) and esterified neem oil (TNO) Characterization

2.3.1 Catalyst characterization

Bucker X-ray D8 advance diffractometer was used to gather powder X-ray diffraction information for structural analysis. For X-ray radiation source, a Cu Kα (λ = 0.154 nm, 45 kV, 40 mA) anode was used, ranging 2θ between 2º and 90º with 0.5 s/step scan rate and 0.05 increment.

Surface analyzer device (Beckman-Coulter; Model: SA3100) was used to measure BET surface area, average pore measurement and pore volume (t-plot strategy) by physical adsorption-desorption of N_2 at the boiling point (77 K). Preceding the examination, Mg-N_{HAp} and N_{HAp} were subjected to a preheating for 90 min at 423 K under vacuum.

A thermal analyzer (NETZSCH: STA449F3 Jupiter) was used for the thermogravimetric analysis of the powder sample. Argon was passed through the instrument with a heating rate of 10 K min^{-1} using a ceramic crucible up to 1000 °C.

A scanning electron microscope (JEOL-JSM-6390LV) furnished with an EDAX PV 9760 detector for Energy Dispersive X-ray spectroscopy (EDX) was used to investigate nearby chemical arrangement. The samples were dispersed in methanol and deposited on an aluminium foil before mounting on sample holder. It was then coated with Gold-Palladium to make the specimen fit for microstructures investigations.

2.3.2 RNO and TNO characterization

The Acid Number of raw neem oil (*Azadirachta indica*) and esterified product was determined by colorimetric titration as per ASTM D974 [13] and saponification number of raw oil was calculated as per ASTM D5558.[14] The acid number and saponification value of RNO was found to be 23.8 mg KOH g^{-1} RNO and 190 mg KOH g^{-1} RNO.

Fourier transform infrared spectroscopy (FTIR) provides information with respect to various functional groups present in the sample. DRS connected with Excalibur Bio-Rad spectrophotometer (Model FTS 3500 GX) FTIR analyzer was utilized for the same. The IR range was between 400 and 4000 cm^{-1} at a scan rate of 40 and at a step size of 4 cm^{-1}.

2.4 Procedure for esterification of neem oil using Mg-N_{HAp}

Activity of Mg-N_{HAp} was studied by esterification of neem oil in a batch reactor having conventional heating framework. For a standard analysis, 30 g of neem oil, methanol and catalyst (2 wt. %) were taken in a 3-necked glass reactor of 1 L volume and was heated up to 70 °C and then agitated for a particular time period. After that the entire reaction mixture was transferred to a rotavapor for removing excess methanol. The reaction mixture was then centrifuged to separate the catalyst and the mixture was kept in a separating funnel overnight to separate the glycerol produced during the reaction. The methyl ester yield was calculated by gas chromatography.

Following the standard method, effect of oil to methanol ratio and catalyst loading on methyl ester yield with respect to reaction time was also studied. To study the kinetics during the reaction progress, small volume of samples was withdrawn negligible to the whole reaction mixture. The methyl ester yield was noted at regular interval of time.

2.5 Reaction kinetics study of the process

The esterification reaction is reversible and the stoichiometric relation between reactant and product is presented below.

$$fa + me \Leftrightarrow fame + w \qquad (1)$$

where *fa*, *me*, *fame* and *w* are presenting fatty acid present in oil, methanol, fatty acid methyl ester and water.

To fit the data in the kinetic model few assumptions were made, as given below.

- In the whole reactant mixture, fatty acid content was limiting and methanol content was in excess.
- The esterification reaction is a heterogeneous process, however the stirring rate is adequate to overcome the diffusion limitation in between reactive species and catalyst.[15]

Considering the above, the generalized rate equation can be written as,

$$-r_f = -dC_{fa}/dt = k_f C_{fa} C_{me} - k_b C_{fame} C_w \qquad (2)$$

where C_{fa}, C_{me}, C_{fame}, C_w are the concentration of fatty acid in neem oil, methanol, fatty acid methyl ester and water. k_f is forward rate constant and k_b is backward rate constant.

So, according to 1st assumption, $C_{me} \approx C_{me_0}$

Thus, Equation 2 can be written as,

$$-dC_{fa}/dt = k_f' C_{fa} - k_b C_{fame} C_w \quad (3)$$

If χ_{fa} is the fatty acid conversion, C_{fa_0}, C_{fame_0}, C_{w_0} are initial concentrations of respective reactants then C_{fa}, C_{fame}, C_w can be expressed as,

$$C_{fa} = C_{fa_0}(1-\chi_{fa}) \quad (4)$$

$$C_{fame} = C_{fame_0} + C_{fa_0}\chi_{fa} \quad (5)$$

$$C_w = C_{w_0} + C_{fa_0}\chi_{fa} \quad (6)$$

As initially $C_{fame_0} = C_{w_0} = 0$, C_{fame} and C_w can be written as $C_{fame} = C_{fa_0}\chi_{fa}$ and $C_w = C_{fa_0}\chi_{fa}$.

Now equation (3) can be expressed as,

$$C_{fa_0} d\chi_{fa}/dt = k_f' C_{fa_0}(1-\chi_{fa}) - k_b {C_{fa_0}}^2 {\chi_{fa}}^2 \quad (7)$$

$$\Rightarrow d\chi_{fa}/dt = k_f' - k_f'\chi_{fa} - k_b C_{fa_0}{\chi_{fa}}^2 \quad (8)$$

When equilibrium state is reached, then $d\chi_{fa}/dt = 0$.

Equation (8) thus becomes,

$$k_f'(1-\chi_{fa_e}) = k_b C_{fa_0}{\chi_{fa_e}}^2 \quad (9)$$

$$\Rightarrow K_e = \frac{k_f'}{k_b} = \frac{{\chi_{fa_e}}^2}{1-\chi_{fa_e}} C_{fa_0} \quad (10)$$

where K_e is the equilibrium constant and χ_{fa_e} is the fatty acid conversion at equilibrium state.

Now, Equation (8) is rearranged as

$$\frac{d\chi_{fa}}{k_f'(1-\chi_{fa})-\frac{k_f'}{K_e}\chi_{fa}^2 C_{fa_0}} = dt \qquad (11)$$

$$\Rightarrow \frac{d\chi_{fa}}{k_f'\left(1-\chi_{fa}-\frac{C_{fa_0}}{K_e}\chi_{fa}^2\right)} = dt \qquad (12)$$

$$\Rightarrow \int_0^{\chi_{fa}} \frac{d\chi_{fa}}{1-\chi_{fa}-p\chi_{fa}^2} = k_f' dt \qquad (13)$$

where $p = \frac{C_{fa_0}}{K_e}$

$\int_0^{\chi_{fa}} \frac{d\chi_{fa}}{1-\chi_{fa}-p\chi_{fa}^2}$ vs t is plotted and by linear fit the k_f' can be calculated.

The rate of esterification reaction is higher at lower activation energy. Hence the reaction temperature effect on kinetic model was studied by using Arrhenius equation which is listed as:

$$k_f' = Ae^{-\left(E_a/RT\right)} \qquad (14)$$

where E_a is activation energy (kJ mol^{-1}), A is Arrhenius constant, R is universal gas constant (8.314 J K^{-1} mol^{-1}) and T (K) is reaction temperature. So to study the effect at varying temperature, equation (14) can be re written as:

$$\ln k_f' = -E_a/RT + \ln A \qquad (15)$$

3. Results and Discussions

3.1 Characterization of Mg-N_{HAp} catalyst

XRD patterns of N_{HAp} and Mg-N_{HAp} are delineated in Fig. 1. Well-resolved characteristic peak of most elevated intensity for HAp was acquired at 2θ value of 31.77° corresponding to 211 planes. The phase formed was clear and matches well with standard pattern reported in literature.[16] The standard corresponding plane for HAp (*viz.* 100,101, 200, 002, 211, 202, 301, 130, 131, 113, 203, 222, 132, 321, 004, 240, 241, 502, 323, and 511) were well observed in case of the synthesized catalyst. The diffraction peak at 2θ = 62.97° with plane 502 corresponds to the Mg support as registered on the XRD patterns (Fig. 1).

The principal evidence for framing of N_{HAp} was in the form of a strong complex broad FTIR band (Fig. 2) focused at about 1000-1120 cm^{-1} because of asymmetric stretching mode of vibration for PO_4 group.[17] The band at 570 cm^{-1} corresponds to P-O stretching vibration of the PO_4 group. As a major peak of phosphate group, the vibration peak could be distinguished in the region between 1120-960 cm^{-1} for both N_{HAp} and Mg-N_{HAp}, which were due to P-O asymmetric stretching of PO_4^{3-}. Many of the compounds can be acknowledged to be analogs of ethers, especially when an alkoxy group was available, featuring the P-O-C linkage at 1240 cm^{-1}. In case of Mg-N_{HAp} the bands at 780-980 cm^{-1} and the peak in the range of 900-1200 cm^{-1} were resulted due to the peroxide formation (M-O-O-M) and the M-O-M bonding respectively.[18]

Fig. 3 shows a typical Nitrogen adsorption-desorption isotherm of N_{HAp} and Mg-N_{HAp}. The isotherms display a type IV curve with a hysteresis loop which corresponds to mesoporous materials. N_{HAp} and Mg-N_{HAp} have BET surface areas of 10.865 m^2 g^{-1} and 134.1 m^2 g^{-1} respectively. Different types of surface area analysis are classified in Table 1. Fig. 3 (in side)

shows a plot of varying pore volume distribution with reference to pore diameter (nm). The total pore volumes were found to be 0.0894 cc g^{-1} and 0.45 cc g^{-1} for N_{HAp} and Mg-N_{HAp} respectively. It can be seen from the Table 1 that, the BJH pore volumes were close to the BET pore volumes for both the samples. Further, it was confirmed that the grafting of Mg on N_{HAp} has significantly increased the BET surface area as well as pore volume.

The morphologies of N_{HAp} and Mg-N_{HAp} are presented in Fig. 4 (a), (b) and Fig. 4 (c), (d) respectively. These SEM micrographs gave understanding into the structure with respect to pore sizes and distribution. The surface of N_{HAp} is almost plane and less porous. However, grafting of Mg followed by calcination at 650 °C led to surface roughness and porous formation. As can be seen from the micrographs, surface morphologies of the Mg-N_{HAp} appears as a polycrystalline material. Fig. 4 (d) shows the porous structure is uniform however, the it was observed to be slit like. The calcination at 650 °C resulted in decomposition of carbonate which helped in forming uniform pores. Hence, the surface area as well as the pore volume was higher in case of Mg-N_{HAp} than N_{HAp} which was evident from the BET results. The EDX analysis of Mg-N_{HAp} showed the presence of C (7.89%), O (43.83%), Mg (19.77%), P (14.13%), Ca (17.37%). The wt. % analysis confirmed the oxide formation of Ca and Mg.

Fig. 5 demonstrates the TGA analysis of N_{HAp} and Mg-N_{HAp}. In case of N_{HAp}, initial weight loss of 6.84% occurred in between the temperature regime of 90 °C to 150 °C because of the evaporation of water molecules. After that the weight loss was found to be about 35% which was due to the decomposition of carbonate as mentioned below.

$$CaCO_3 \rightarrow CaO + CO_2 \qquad (16)$$

However, in case of Mg-N_{HAp}, the initial weight loss was only about 3.48% (within 150 °C). Moreover, no crest was found within a temperature region of 150 °C to 1000 ºC and the reported weight loss was only 7.5 %. The TGA curve within this specified temperature range was thought to be the aftereffect of continuous de-hydroxylation of Mg-N_{HAp} powder. It is clear from the TGA that the total weight loss at 1000 °C was 10.98 % for Mg-N_{HAp} compared to 41.7% for N_{HAp}. Thus, it was confirmed that Mg grafting resulted in a more stable Mg-N_{HAp}.

3.2 Parametric effects on Methyl ester yield

3.2.1 Effect of oil to methanol ratio on methyl ester yield at constant weight of catalyst

The usual esterification reaction is conducted in excess of methanol, which leads to forward reaction because of reversibility. In order to analyze the outcomes of oil to methanol ratio on the reaction, few experiments were conducted with molar ratio of 1:5, 1:10, 1:15, 1:20, and 1:25 as shown in Fig 6. It shows the effect of neem oil to methanol molar ratio on methyl ester yield with reference to reaction time. Significant effect was clearly observed affecting the methyl ester yield. The time required to reach highest yield at lower concentration of Mg-N_{HAp} (2 weight% of oil) and lower oil to methanol ratio (1:5), was approximately 250 minutes. But with increase in oil to methanol ratio the time required to reach highest conversion gradually decreased to 135 minutes.

The concentration of methanol has dominant role during esterification reaction. The methyl ester yield was increased significantly with the addition of methanol. Nevertheless, higher concentration of methanol may adsorb on the catalyst active sites because of which the esterification process inhibited. As shown in the Fig. 6 the oil to methanol molar ratio was

increased by keeping catalyst loading constant in the reaction system. It can be seen that after 1:15 oil to methanol ratio the reduction in conversion was clearly observed.

3.2.2 Effect of varying weight loading of catalyst on methyl ester

The methyl ester yield vs. reaction time data were obtained at varying Mg-N_{HAp} weight % but at constant oil to methanol ratio (1:15) and reaction temperature (70 °C) are presented in Fig. 7. It shows the percentage increase in methyl ester yield with and without catalyst. In the figure, the 0% Mg-N_{HAp} shows that the whole reaction was conducted without catalyst. Further, the catalyst loading was gradually increased by 1% to see the catalytic effect on the yield obtained. The interaction between catalyst and reactant was more obvious at early stage of the reaction. It was evident from the analysis that without using catalyst the equilibrium conversion was achieved after three and half hour. Also it can be clearly noted that the time required to reach equilibrium conversion has gradually been decreased with increase in Mg-N_{HAp} weight%. There is increase in reaction rate perhaps due to the increase in number of active sites inside the reaction chamber. Highest yield of 96.7% was observed when the Mg-N_{HAp} loading increased to 6%. Methyl ester yield was increased from 48.7% (0% Mg-N_{HAp}) to 95% (6% Mg-N_{HAp}) in 135 minutes. The gradual increase in yield can be attributed to the increase in number of active catalytic sites available in the reaction chamber.

3.2.3 Effect of reaction temperature on the methyl ester yield

Reaction temperature plays an important role during esterification reaction. The effect of varying reaction temperature on methyl ester yield was shown in Fig. 8. The rate of reaction increased with temperature, although at equilibrium state the concentrations remain same for all the temperature.[19] The reactions were conducted at 60 °C, 70 °C, 80 °C and 90 °C in presence

and absence of catalyst at fixed 1:15 oil to methanol ratio. A significant and rapid rise in methyl ester yield was clearly observed with increase in reaction temperature. This is due to the higher molecular activity and mass transfer which eventually lead to faster reaction rate.

3.3 Evaluation of kinetic rate constant and activation energy of neem oil esterification reaction

Equation (13) shows the reaction kinetic model for the pseudo-first-order reaction. This equation was used for regression analysis of the obtained experimental data at varying catalyst loading and reaction temperature so as to calculate the reaction rate constant. After linearly fitted, the slope i.e. $k_f^{'}$ is listed in the Table 2. It's clearly showing the significant rise in rate with increase in reaction temperature.

The catalyst loading has also significant effect on the forward rate constant, which is explained by the following equation.

$$k_f^{'} = k_{Mg-N_{HAp}} W_{Mg-N_{HAp}} \qquad (17)$$

Where, $k_{Mg-N_{HAp}}$ is the Mg-N_{HAp} loading coefficient and $W_{Mg-N_{HAp}}$ is the weight ratio of catalyst to oil. Following Eq. 17, a graph (Fig. 9) was plotted between forward rate constant vs weight ratio of catalyst to oil. The slope of the plot presents the $k_{Mg-N_{HAp}}$ i.e. 0.575 min^{-1}.

The kinetics parameter of esterification *viz.* rate constant, activation energy (E_a) and pre-exponential factor (A) were calculated from Arrhenius equation. E_a was calculated for two set of reactions separately, first is at 0% Mg-N_{HAp} loading and second at 6% Mg-N_{HAp}. Fig. 10 illustrates a linear correlation between $\ln k_f^{'}$ and 1/T. The slope of the line gives E_a. The final value of E_a and A is enlisted in Table 3. It's clearly showing that the activation energy decreases from 47.86 kJ mol^{-1} to 32.35 kJ mol^{-1} after addition of Mg-N_{HAp}.

3.4 Thermodynamic properties of Mg-N_{HAp} catalyzed esterification

The thermodynamic properties of esterified product were also studied. As per Van't Hoff equation, the Gibbs free energy (ΔG in kJ mol^{-1}) is expressed as follows:

$$\Delta G = -RT \ln K \qquad (18)$$

Where R is universal gas constant (8.314 J K^{-1} mol^{-1}), T is temperature in Kelvin and K is equilibrium constant.

Considering change in enthalpy and entropy with temperature constant, ΔG can be written as

$$\Delta G = \Delta H - T\Delta S \qquad (19)$$

Now combining both equation (18) and (19),

$$\ln K = \left(\frac{-\Delta H}{RT}\right) + \left(\frac{\Delta S}{R}\right) \qquad (20)$$

$$\Rightarrow -R \ln K = \left(\frac{\Delta H}{T}\right) - \Delta S \qquad (21)$$

After plotting $-R \ln K$ vs $\frac{1}{T}$ and linearly fitting the values of ΔH, ΔS can be calculated.

A linear correlation between $-R \ln K$ vs $\frac{1}{T}$ is shown in Fig. 11 (a) for both 0% Mg-N_{HAp} and 6% Mg-N_{HAp} loading. The slope and intercept of the corresponding plots represents enthalpy (ΔH) and entropy (ΔS) of the reaction. The enthalpy (ΔH) for 0% and 6% Mg-N_{HAp} loading was found to be 104.06 kJ mol^{-1} and 49.3 kJ mol^{-1} at 333K. Fig. 11 (b) shows the Gibbs free energy variation for the esterification reaction with and without catalyst for temperature ranging from 333K to 363K. The trend line shows that the reaction is continuous process.

3.5 FTIR results of purified and esterified neem oil

Fig. 12 presents the graph in between wave number (cm^{-1}) and Transmittance (%) for esterified neem oil produced at constant reaction temperature (70 °C), oil to methanol ratio (1:30) and Mg-N_{HAp} weight % (2%). At first it is clear from the figure that alkane is present without phosphorous and sulfur. This confirms that leaching of catalyst didn't occur and it was separated clearly. Also a C=O group is identified at 1742 cm^{-1} which refers to ester. Other wavenumbers and corresponding functional groups are marked in the figure.

3.6 Comparison of earlier reported work with present work using hydroxyapatite based catalyst for esterification

Table 5 reported a comparison of different natural and synthetic hydroxyapatite based heterogeneous catalysts and their methyl ester yield at different operating parameters reported in literature.[2, 7, 20-22] It can be observed from the data that all the catalyst developed possess very less BET surface area in comparison to present developed catalyst. But Al_2O_3/H_3PO_4 (synthetic hydroxyapatite) has very good surface area i.e. 120 m^2 g^{-1}. Jazie et al. tried to produce methyl ester from peanut oil using animal bone powder and observed more than 80 % of yield with gradual increase in reaction time period. However, reaction time was bit higher than present study. They also have studied methyl ester yield of rapeseed oil using the same catalyst and found above 85% yield. In this case also reaction time period as well as methanol to oil ratio was extensively high.[20] Chakraborty and RoyChowdhury tried to produce oleic acid ethyl ester using Cu grafted fishbone derived hydroxyapatite. The catalyst has very low surface area. In spite of having lower surface area the yield obtained was good. However, the effect of yield with and without metal grafting was not discussed.[7] Xie et al. also produces methyl ester from rapeseed oil using biont shell without metal support. The results were much promising considering all the

parameters except catalyst loading.[21] Obadiah et al. used palm oil to produce methyl ester, for which the yield was above 80% at 15 wt. % catalyst loading and 4 h reaction time period. They observed above 95% conversion when catalyst wt. % loading was 20%, which is very high if the same process is considered in a large scale.[2] Araujo et al. used synthetic hydroxyapatite with Al metal support for esterification of Oleic acid. They observed highest conversion of 95% within 1 h, but only demerit in the work was reaction temperature i.e. 350 °C.[22] Thus, observing all the positive and negative aspects of the proclaimed works, the present experiments were conducted. It is confirmed from the comparison that such types of reactions can give promising results using the present developed catalyst.

3.7 Reusability study of Mg-N_{HAp} during esterification

Reusability of Mg-N_{HAp} was studied by multiple repetition (5 times) of esterification experiments at constant oil to methanol ratio (1:15), reaction temperature (70 °C) and catalyst loading (6 wt. %). After each reaction, the final mixture was centrifuged to remove the catalyst. Then it was regenerated by washing with methanol several times and then dried for 2 h at 110 °C. The regeneration process was continued for 5 times after each run. From Fig. 13, it can be inferred that the yield after regeneration doesn't vary significantly up to 5^{th} regeneration. After 5^{th} regeneration the yield was decreased to 91.5% from 96.7% after 160 min. The low variation in yield after regeneration thus affirms the stability of Mg-N_{HAp}.

4. Conclusion

An active, reusable solid catalyst was prepared from cooked waste fish bone. Grafting of Mg ion by impregnation followed by calcination resulted in high surface area and pore volume. The method of reusing fishbone waste to prepare catalyst could help waste recycling,

contaminants minimization, cost reduction and making the catalyst environmentally viable. This high efficient and low-cost fishbone catalyst could make the process of esterification economic also. Thus, it can be anticipated that this low-cost catalyst if utilized in a large-scale industrial process of biofuel production, will make the entire process sustainable as well as low cost. Also this work gives a new horizon towards the use of various bio-waste products for heterogeneous catalyst development.

Acknowledgement

Authors acknowledge the analytical facilities i.e. FESEM, EDX, BET, TGA analysis provided by Central Instruments Facility (CIF), IIT Guwahati. Use of XRD facility (procured through FIST Grant No. SR/FST/ETII–028/2010 from Department of Science and Technology, Government of India) at Department of Chemical Engineering, IIT Guwahati is also acknowledged.

Reference

1. T. Rustad, *Electron. J. Environ. Agric. Food Chem.*, 2003, **2**, 458-463.

2. A. Obadiah, G.A. Swaroopa, S.V. Kumar, K. R. Jeganathan and A. Ramasubbu, *Bioresour. Technol.*, 2012, **116**, 512–516.

3. S.M. Best, A.E. Porter, E.S. Thian and J. Huang, *J. Eur. Ceram. Soc.*, 2008, **28**, 1319-1327.

4. T. Leventouri, *Biomaterials.*, 2006, **27**, 3339-3342.

5. J. Venkatesan, B. Lowe, P. Manivasagan, K.H. Kang, E.P. Chalisserry, S. Anil, D.G. Kim and S.K. Kim, *Materials*, 2015, **8**, 5426-5439.

6. K. Sasaki and T. Goto, *Ceram. Int.*, 2014, **40**, 11649-11656.

7. R. Chakraborty and D. RoyChowdhury, *Chem. Eng. J.*, 2013, **215**, 491-499.

8. L.B. Sun, X.Q. Liu, and H.C. Zhou, *Chem. Soc. Rev.*, 2015, **44**, 5092-5147.

9. M. Verziu, B. Cojocaru, J. Hu, R. Richards, C. Ciuculescu, P. Filipc and V. I. Parvulescu, *Green Chem.*, 2008, **10**, 373-381.

10. L.B. Sun, W.H. Tian, and X.Q. Liu, *J. Phys. Chem. C*, 2009, **113**, 19172-19178.

11. C. Xu, D.I. Enache, R. Lloyd, D.W. Knight, J.K. Bartley and G.J. Hutchings, *Catal. Lett.*, 2010, **138**, 1-7.

12. J. Wang, T. Nonami and K. Yubata, *J. Mater. Sci.: Mater. Med.*, 2008, **19**, 2663-2667.

13. A. Baig and F. T. Ng, *J. Am. Oil Chem. Soc.*, 2011, **88(2)**, 243-253.

14. D. T. Englis and J. E. Reinschreiber, *Anal. Chem.*, 1949, **21.5**, 602-605.

15. J. I. Choi, W. H. Hong and H. N. Chang, *Int. J. Chem. Kinet.*, 1996, **28**, 37.

16. J.H.G. Rocha, A.F. Lemos, S. Kannan, S. Agathopoulosa and J.M.F. Ferreira, *J. Mater. Chem.*, 2005, **15**, 5007-5011.

17. H.K. Varma and S.S. Babu, *Ceram. Int.*, vol. 2005, **31**, 109-114.

18. S. Maensiri, P. Laokul and V. Promarak, *J. Cryst. Growth*, 2006, **289**, 102-106.

19. M.G. Kulkarni, R. Gopinath, L.C. Meher, A.K. Dalai, *Green Chem.*, 2006, **8**, 1056-62.

20. A.A. Jazie, H. Pramanik and A.S.K. Sinha, *Mater. Renewable Sustainable Energy*, 2013, **2**, 1-10.

21. J. Xie, X. Zheng, A. Dong, Z. Xiao, and J. Zhang, *Green Chem.*, 2009, **11**, 355-364.

22. L.R.R.D. Araujo, C.F. Scofield, N.M.R. Pastura and W.D.A. Gonzalez, *Mater. Res.*, 2006, **9**, 181-184.

Figure Caption

Fig. 1 X-ray diffraction pattern of N_{HAp} and Mg-N_{HAp}

Fig. 2 FTIR of N_{HAp} and Mg-N_{HAp} showing relevant functional groups

Fig. 3 N_2 adsorption and desorption of N_{HAp} and Mg-N_{HAp}, volumetric distribution (in side)

Fig. 4 SEM images of N_{HAp} (a), (b) and Mg-N_{HAp} (c), (d) showing surface murphology

Fig. 5 Thermogravimetric analysis of N_{HAp} and Mg-N_{HAp}

Fig. 6 Effects on FFA conversion with reference to reaction time at varying oil to methanol ratio

Fig. 7 Effects on methyl ester yield with reference to reaction time at varying catalyst loading

Fig. 8 Effects of methyl ester yield with reference to reaction time at varying reaction temperature for 0% and 6% catalyst loading

Fig. 9 Graph of $k_f^{'}$ vs $W_{Mg-N_{HAp}}$

Fig. 10 Plot showing linear correlation between $\ln k_f^{'}$ and 1/T

Fig. 11 (a) linear correlation between $-R\ln K$ vs $\frac{1}{T}$ (b) Gibbs free energy variation for the esterification reaction for 0% and 6% Mg-N_{HAp} loading

Fig. 12 FTIR of purified and esterified neem oil

Fig.13 Regeneration profile of Mg-N_{HAp}

Table 1: Different surface area (m^2/g) measurements and pore volume (cc/g)

Parameter	Surface Area & Pore Volume		Co-relation Co-efficient	
	N_{HAp}	Mg-N_{HAp}	N_{HAp}	Mg- N_{HAp}
Langmuir Surface area (m^2 g^{-1}) at P_S/P_0=0.9814	5.708	128.45	0.99	0.99
One Point BET Surface Area (m^2 g^{-1}) at Ps/Po=0.3	8.879	131.24	-	-
Adsorbed BET Surface area (m^2 g^{-1})	10.865	134.1	0.97	0.99
Adsorbed t-plot Surface area (m^2 g^{-1})	27.261	136.376	0.98	0.99
Total pore volume (cc g^{-1}) at P_S/P_0=0.9814	0.0894	0.4529	-	-
Total BJH pore volume (cc g^{-1})	0.10882	0.46863	-	-

Table 2: k_f' (min^{-1}) for 0% and 6% Mg-NHAp loading with respective reaction temperature (K) and 1:15 oil to methanol ratio

Reaction Temperature (K)	Oil to methanol ratio	k_f' (min^{-1})	
		Mg-NHAp=0%	Mg-NHAp=6%
333	1:15	0.0135	0.0137
343	1:15	0.0265	0.0179
353	1:15	0.037	0.0244
363	1:15	0.0591	0.0364

Table 3: Activation energy and Arrhenius constant with and without catalyst*

	E_a (kJ mol^{-1})	A
Mg-NHAp=0%	47.86	464167.1
Mg-NHAp=6%	32.35	1575.9

* All the reaction were carried out with 1:15 oil to methanol ratio

Table 4: Enthalpy at varying temperature for 0% and 6% Mg-N_{HAp} loading*

Temperature (K)	ΔH (kJ mol^{-1})	
	0 % Mg-N_{HAp} loading	6% Mg-N_{HAp} loading
333	104.06	49.2
343	107.1	50.7
353	110.03	52.2
363	113.4	53.7

* All the reactions were carried out at oil to methanol molar ratio of 1:15.

Table 5. Methyl ester yields using various natural and synthetic hydroxyapatite based catalysts in vegetable oil/fatty acid esterification and comparison with the present work

Fatty acid/ vegetable oil	Catalyst	BET surface area (m^2 g^{-1})	Reaction process Parameter	Methyl ester yield
Peanut [20]	Animal bone powder	4.01	4 h, 60 °C, 600 rpm	<80%
Oleic acid [7]	Cu/Hydroxyapatite (Fishbone)	16.78	1h, 70 °C, 800 rpm, 0.4 mL min^{-1} ethanol flowrate	<83.57%
Rapeseed [21]	Biont shell	12.64	3h, 70 °C, 600 °C (calcination), 9:1 methanol to oil	<80%
Palm [2]	Waste animal bone	88.53	4h, 65 °C, 800 °C (catalyst calcination), 200 rpm, 15 wt. % catalyst loading	80%
Rapeseed [20]	Animal bone powder	4.01	4h, 60 °C, 24:1 methanol to oil, 600 rpm	85%
Oleic acid [22]	Al_2O_3/H_3PO_4 (Synthetic)	120	1h, 350 °C, 0.15 (mmol acid/g product)	95.5%
Present Work (neem)	Mg/Hydroxyapatite (Fishbone)	131.24	2.25h, 70 °C, 1:15 (oil to methanol), 6 wt.% catalyst loading, 650 °C (calcination)	95%

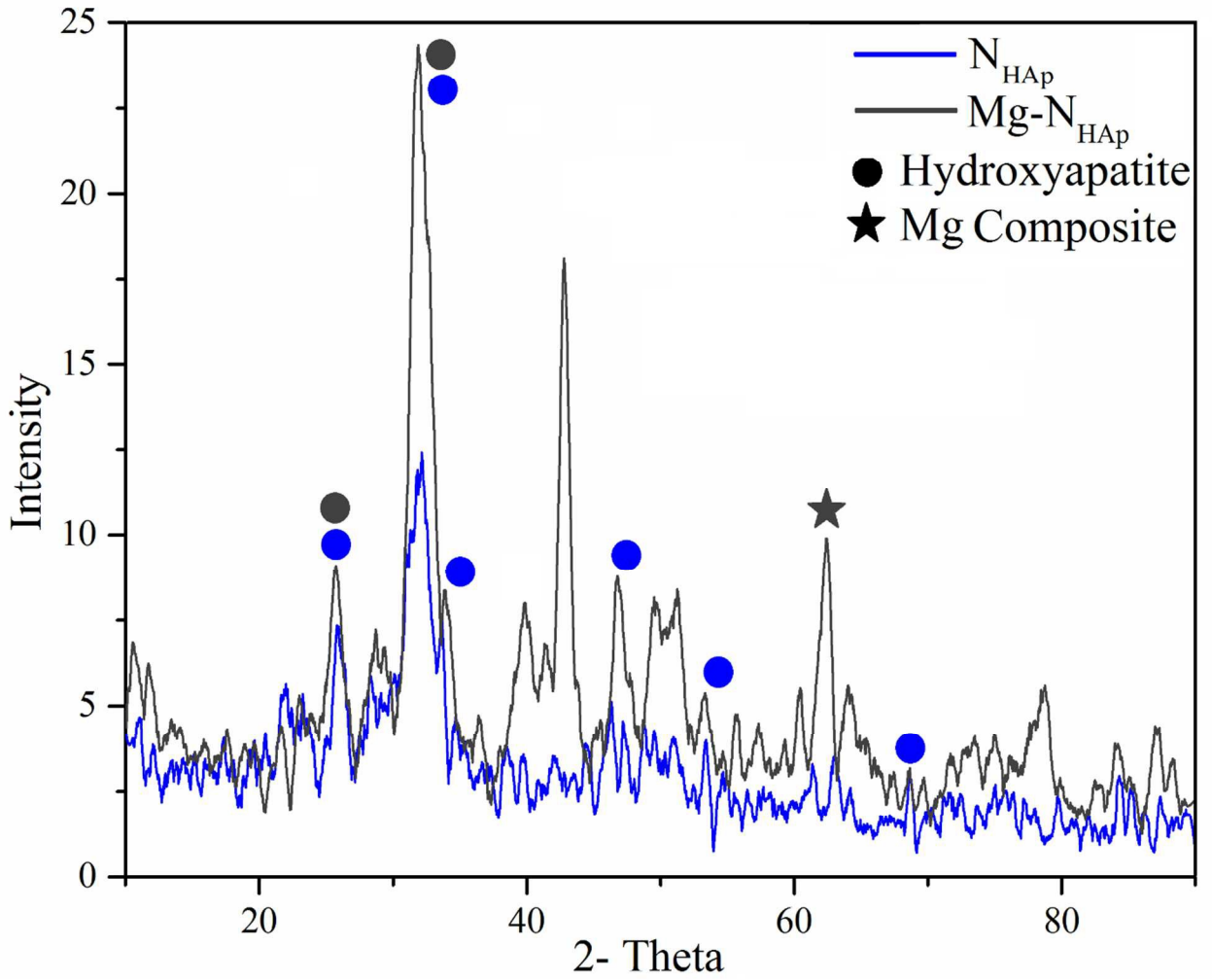

Fig. 1

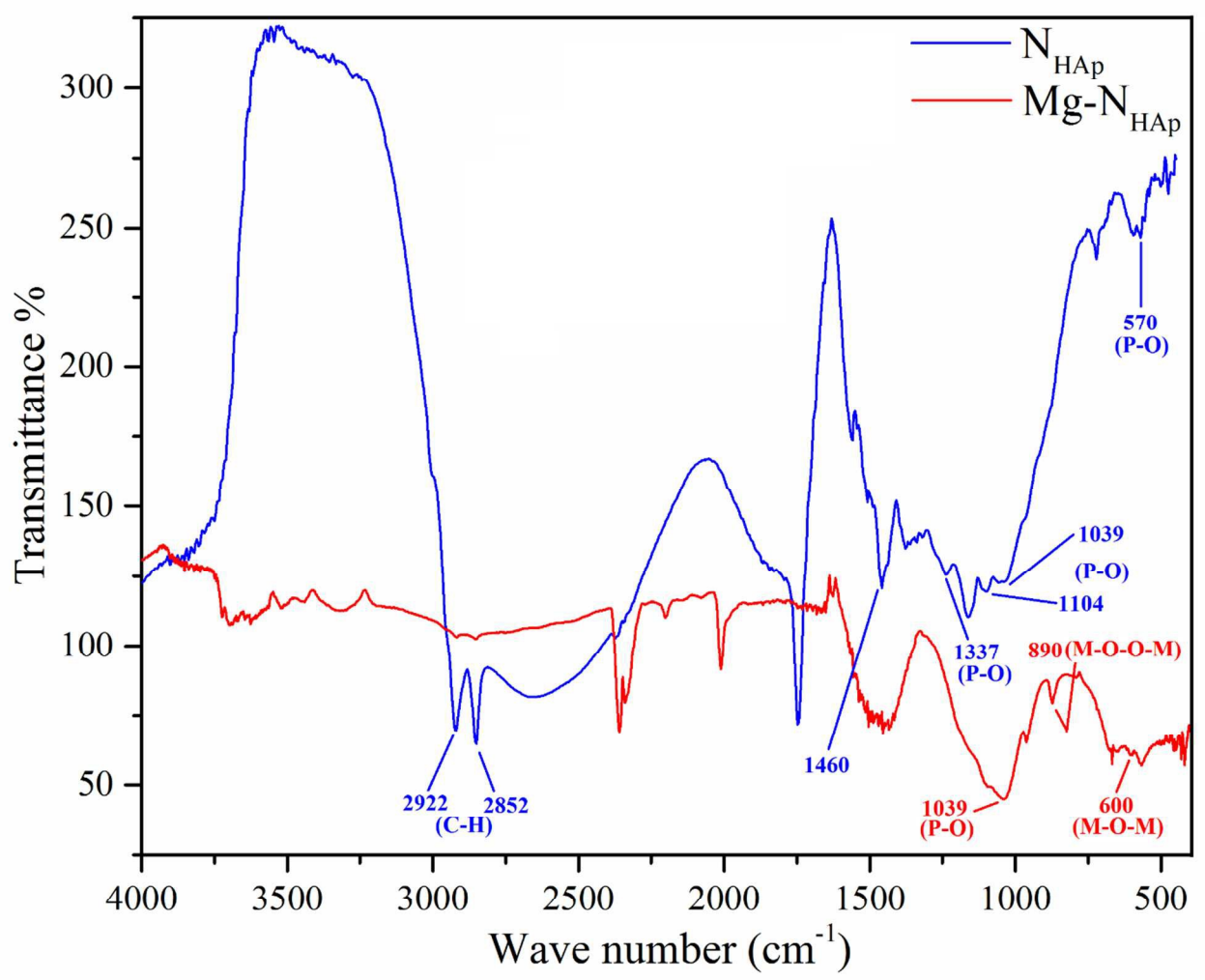

Fig.2

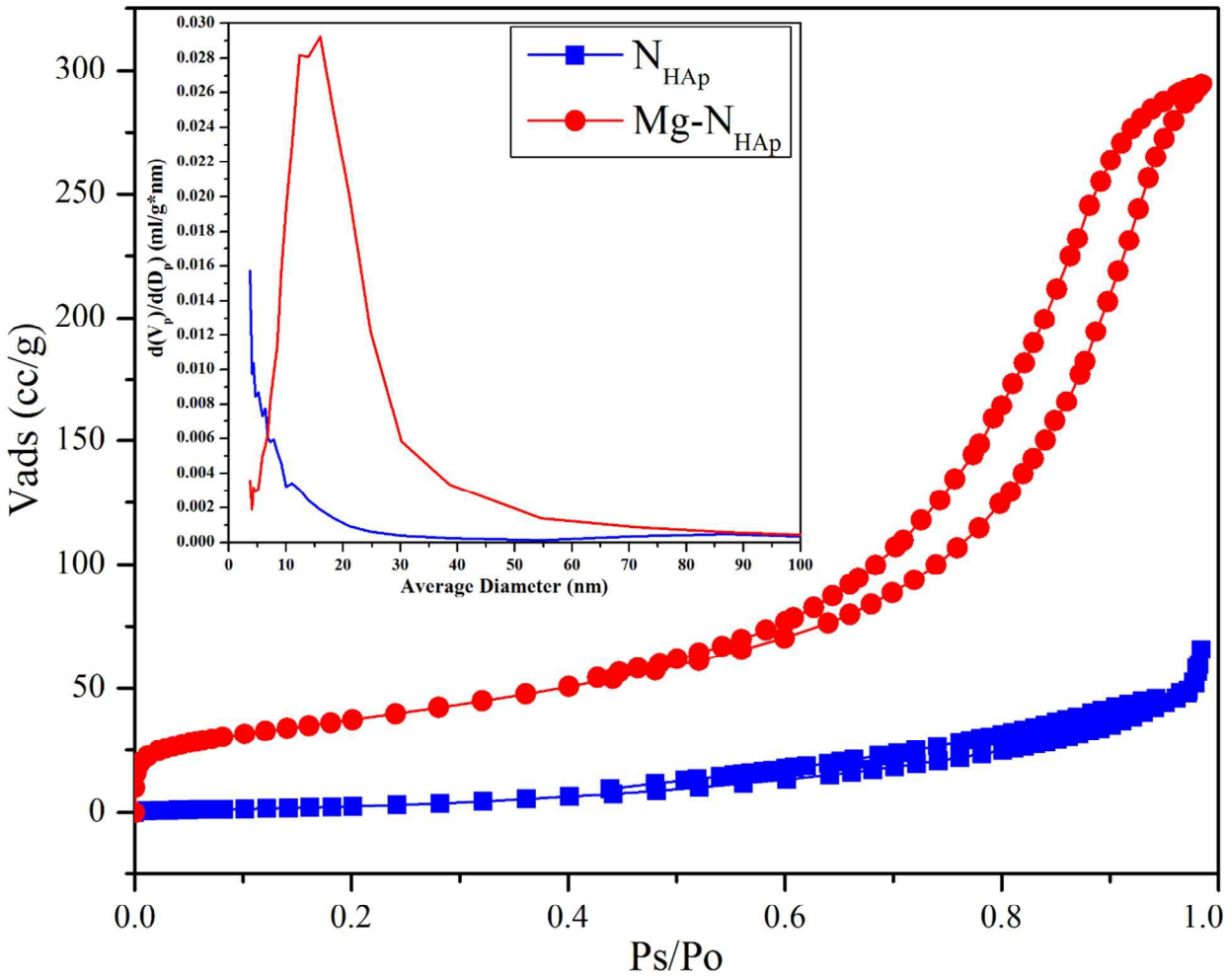

Fig. 3

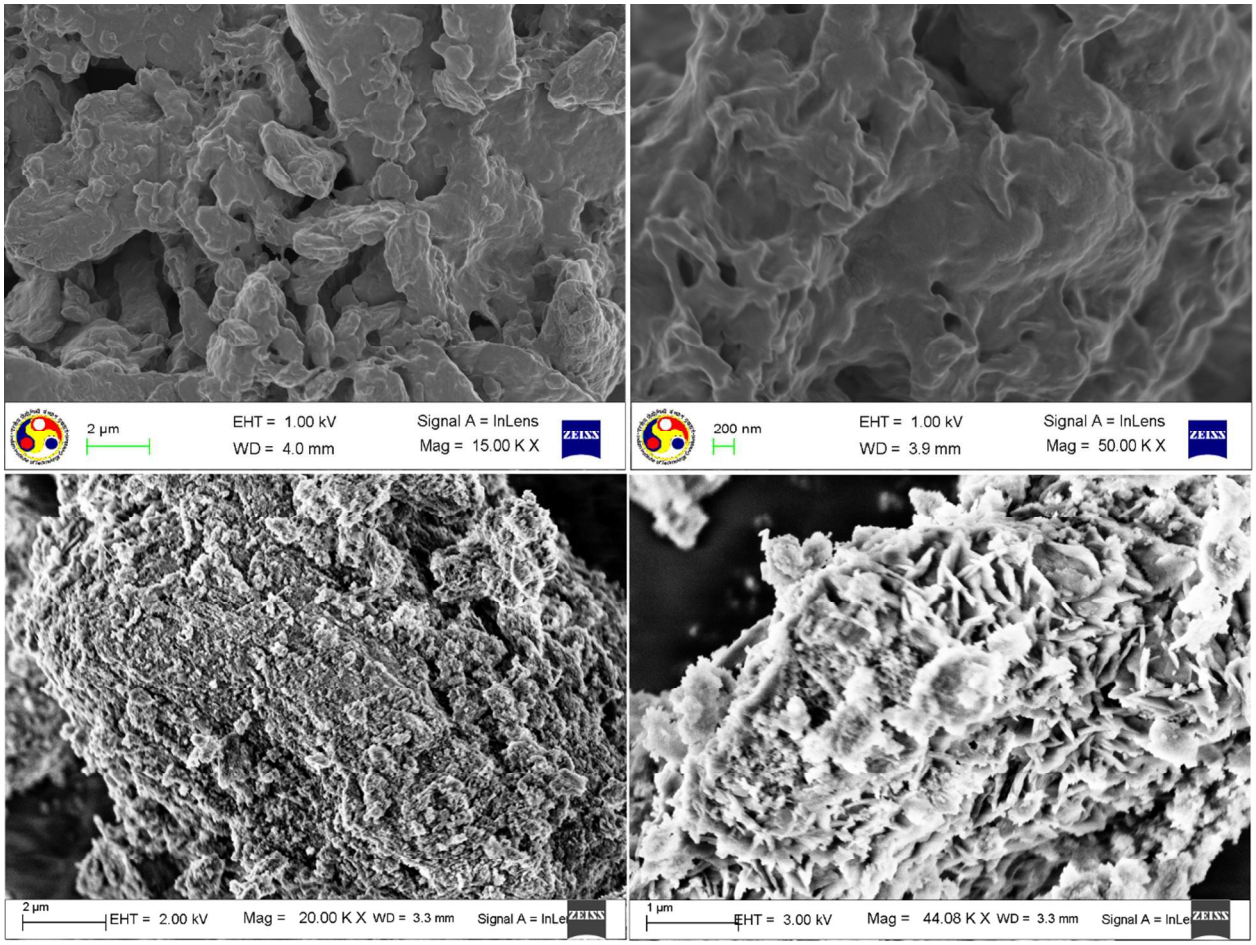

Fig. 4

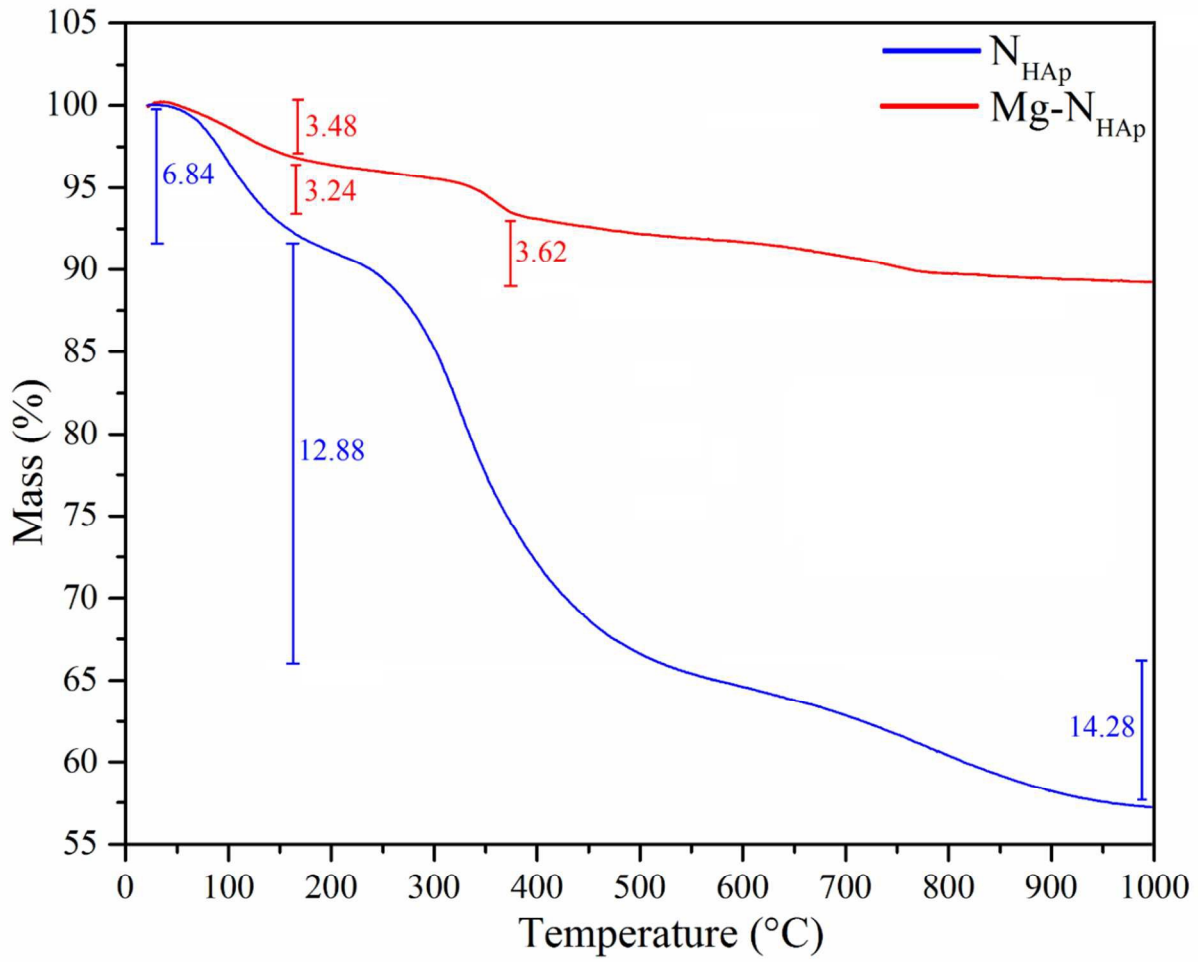

Fig. 5

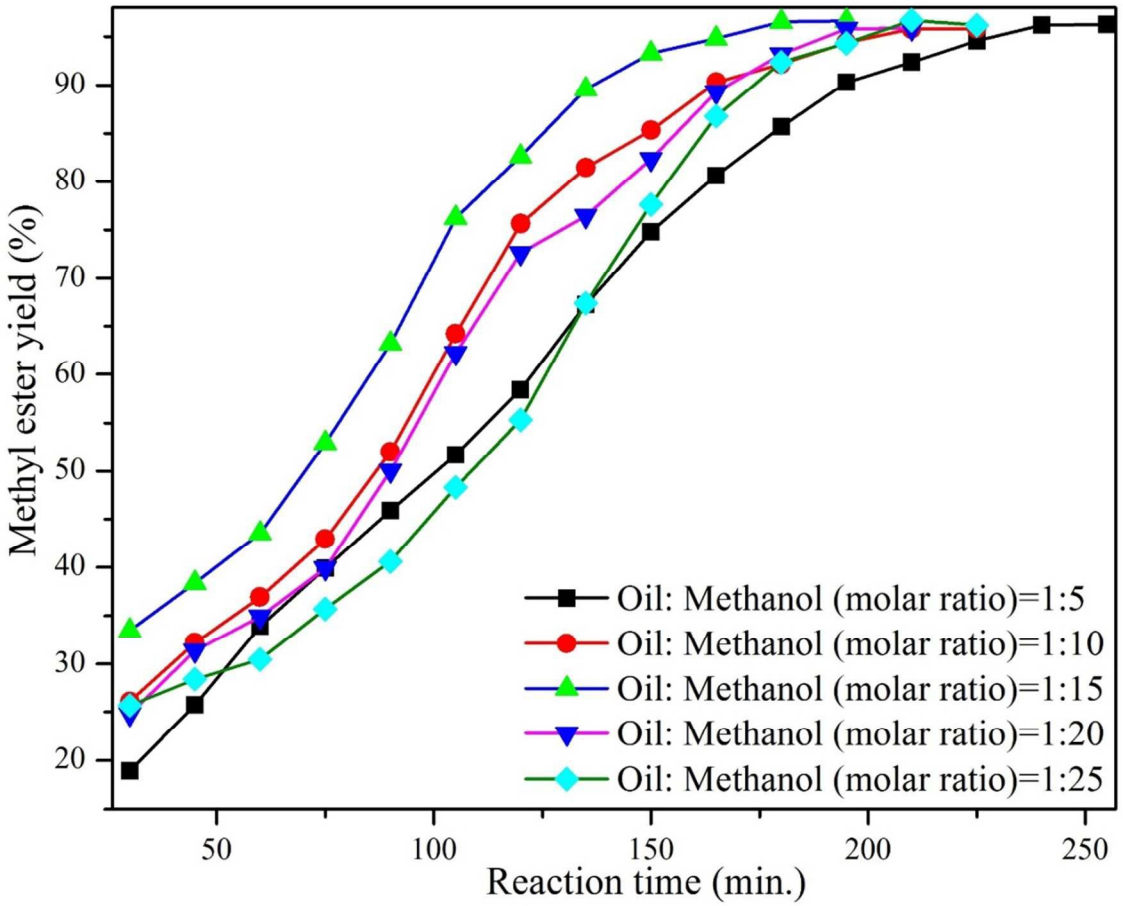

Fig. 6

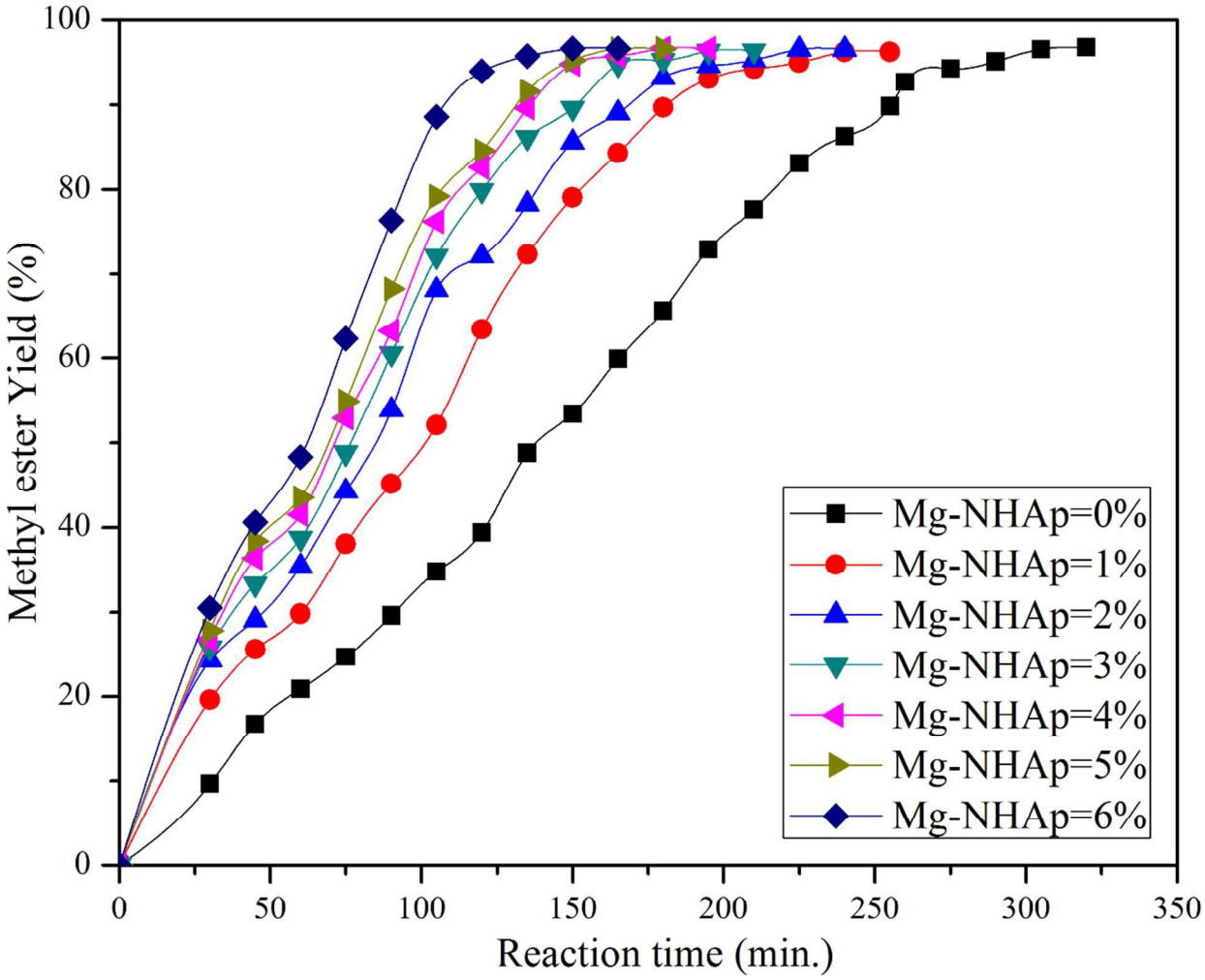

Fig. 7

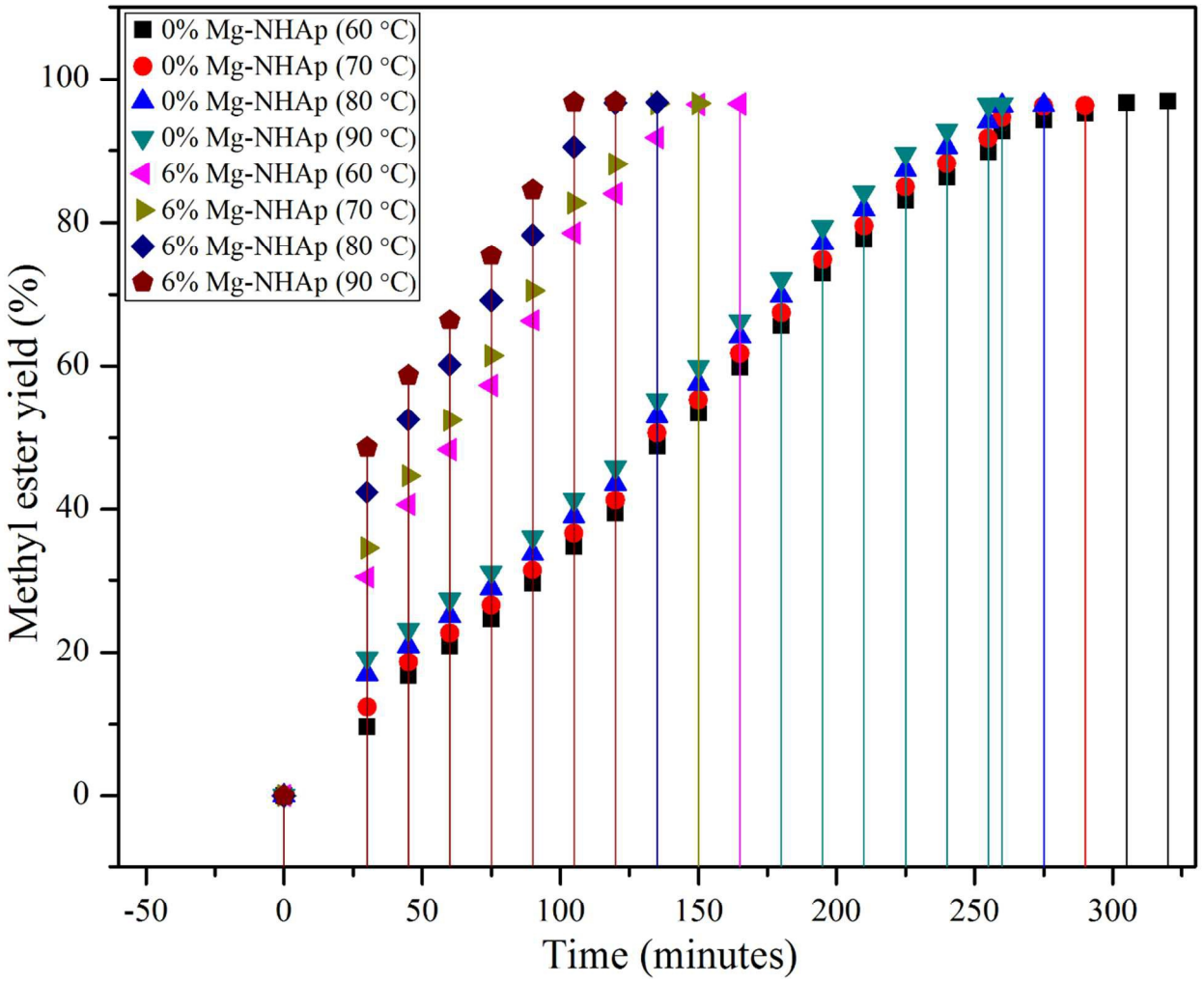

Fig. 8

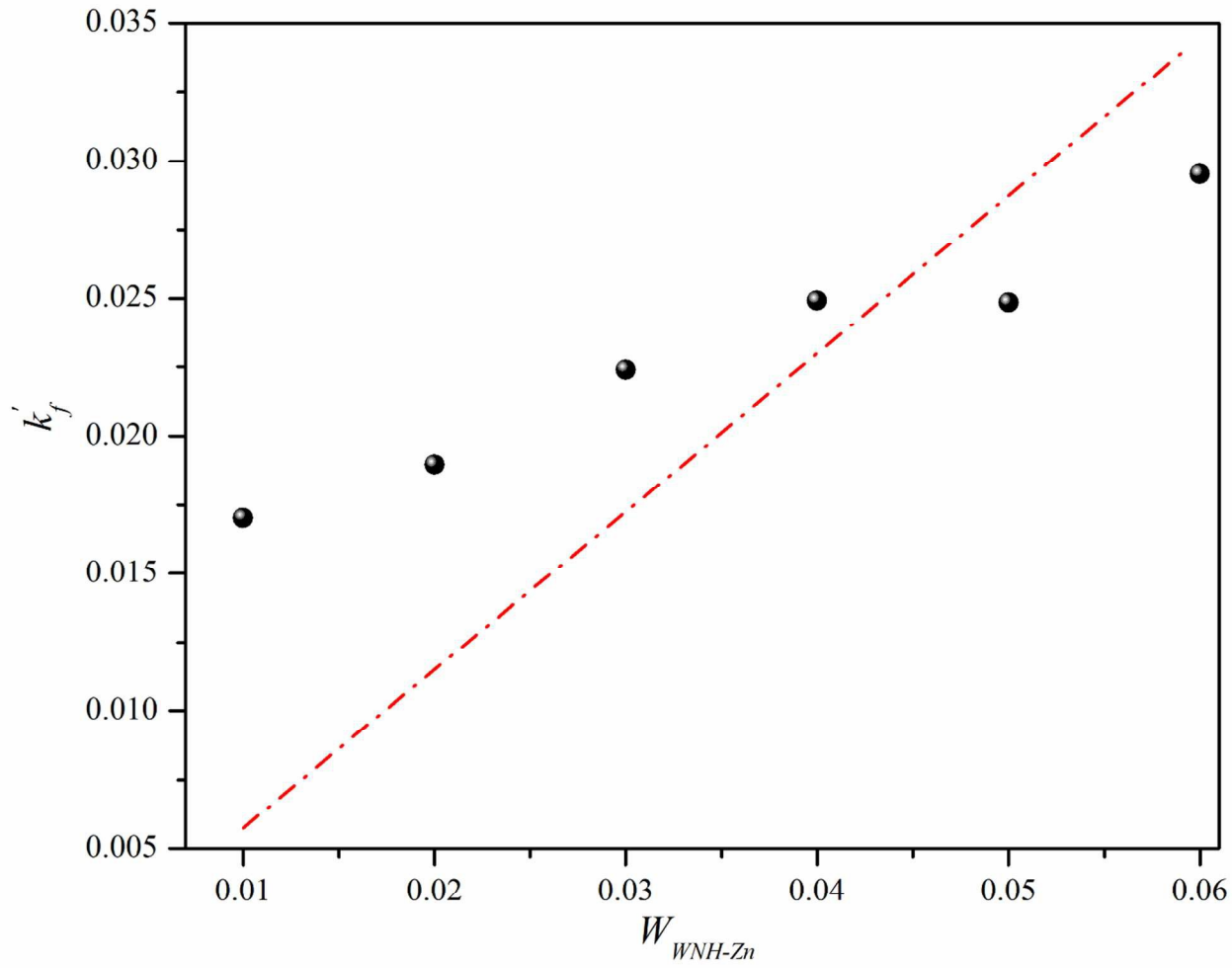

Fig. 9

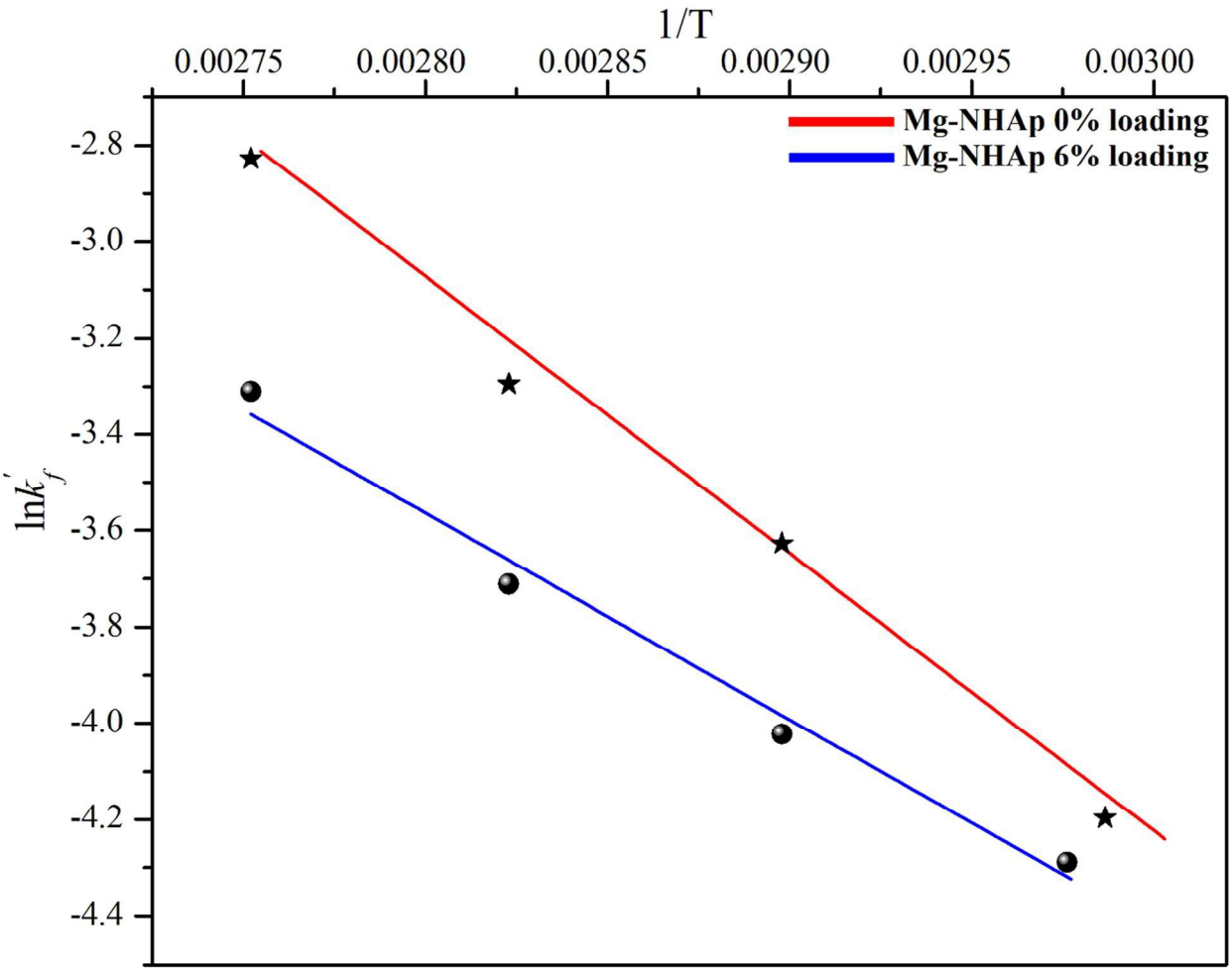

Fig. 10

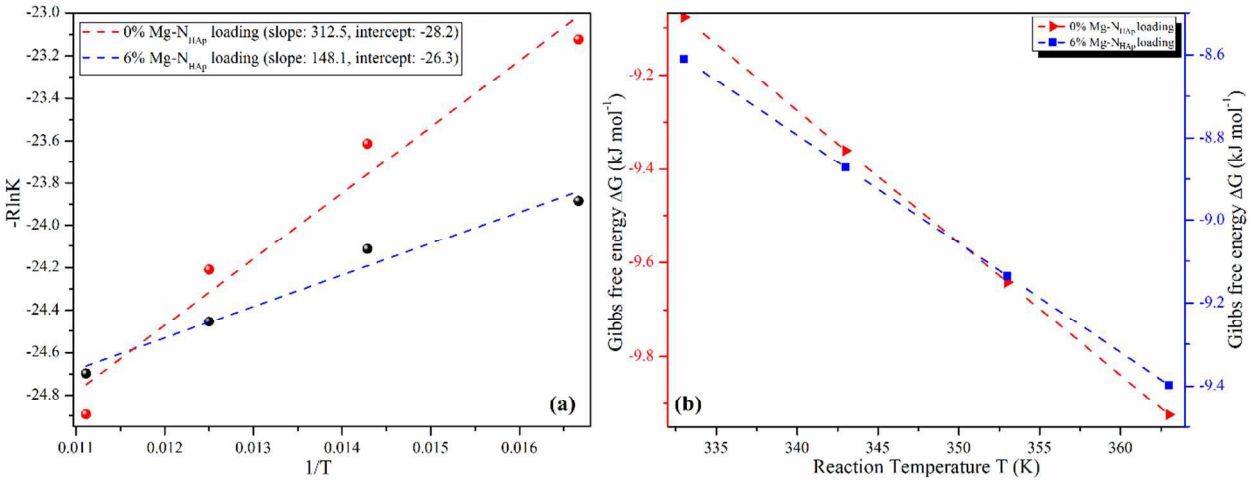

Fig. 11

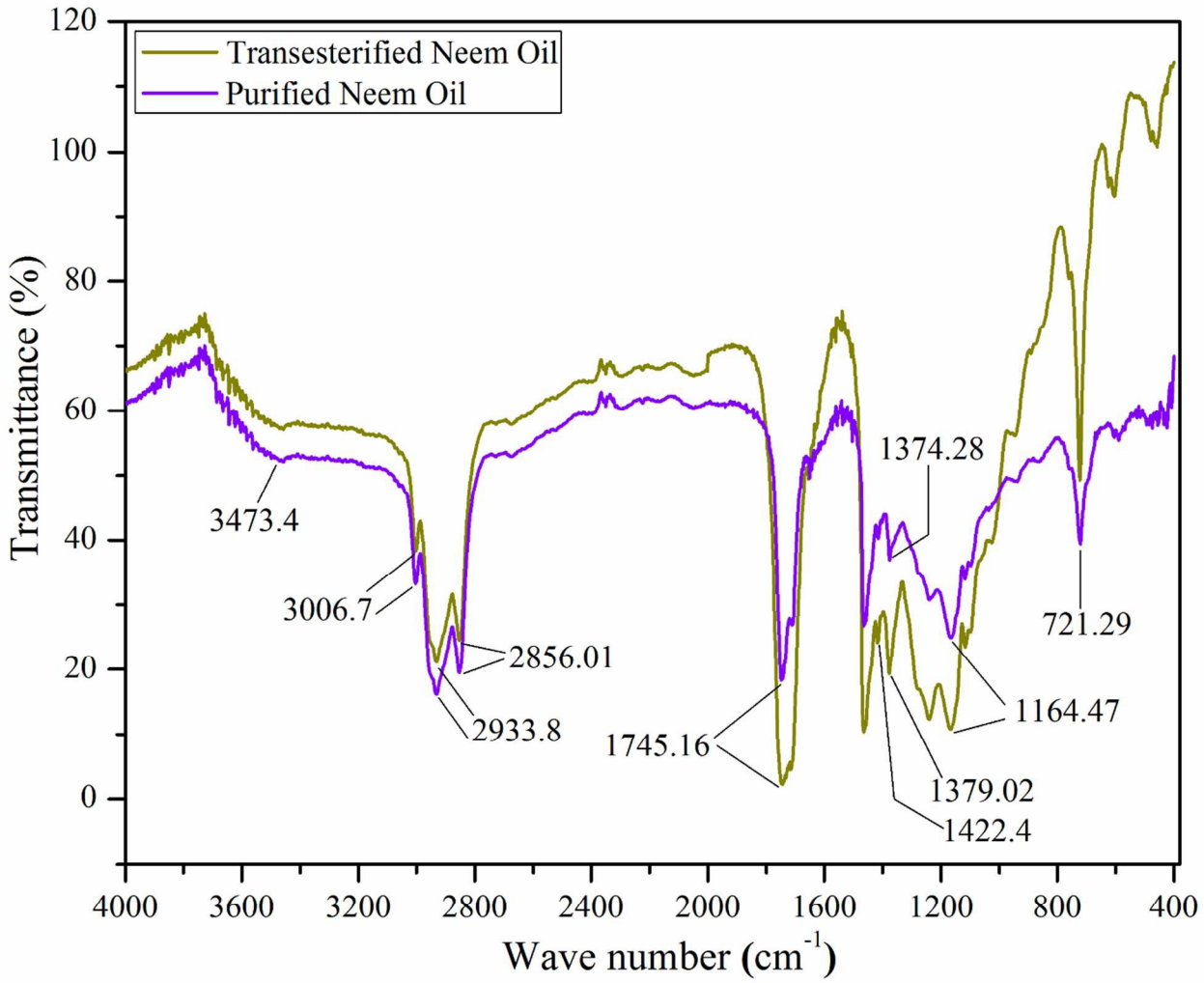

Fig. 12

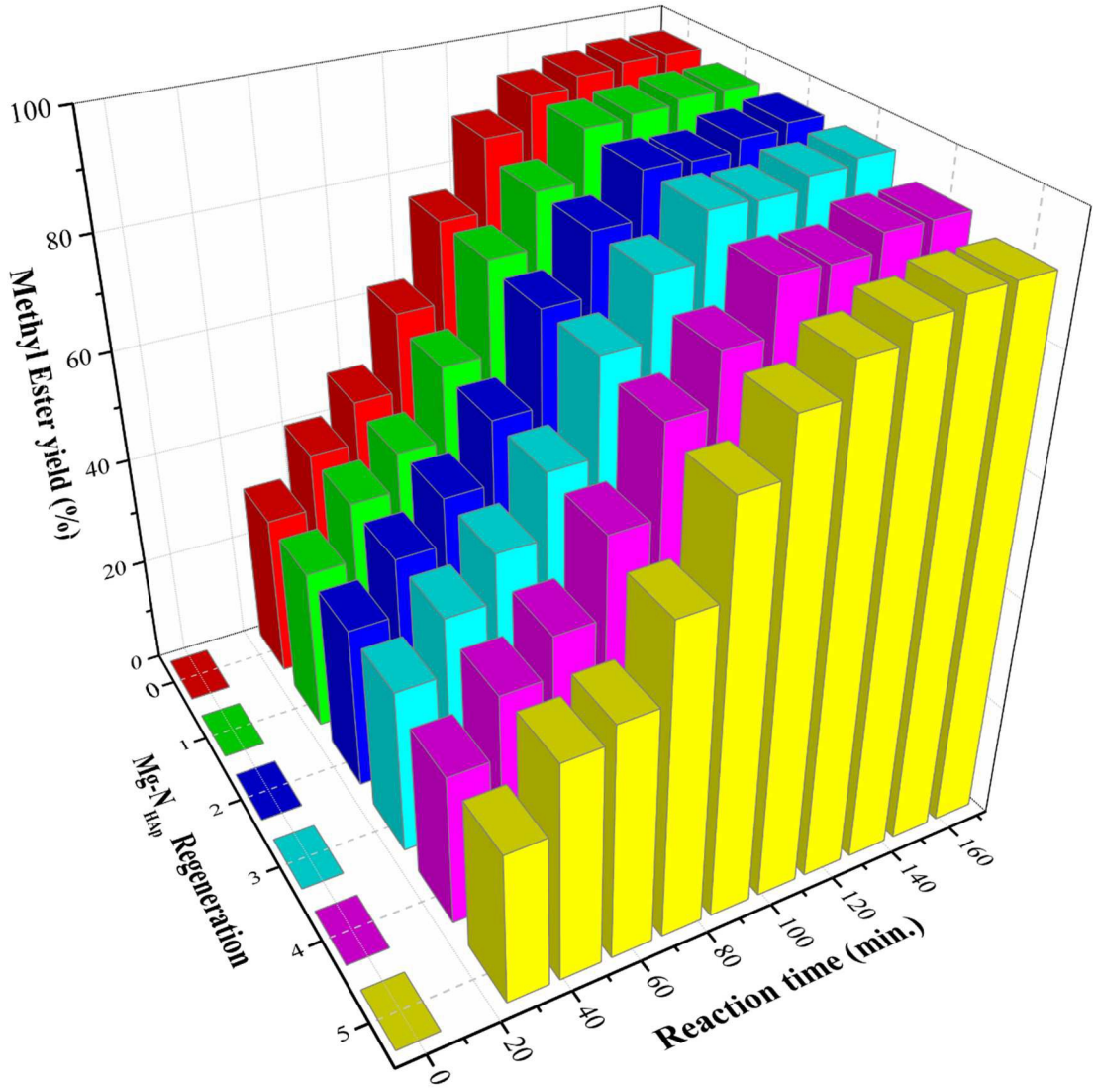

Fig. 13

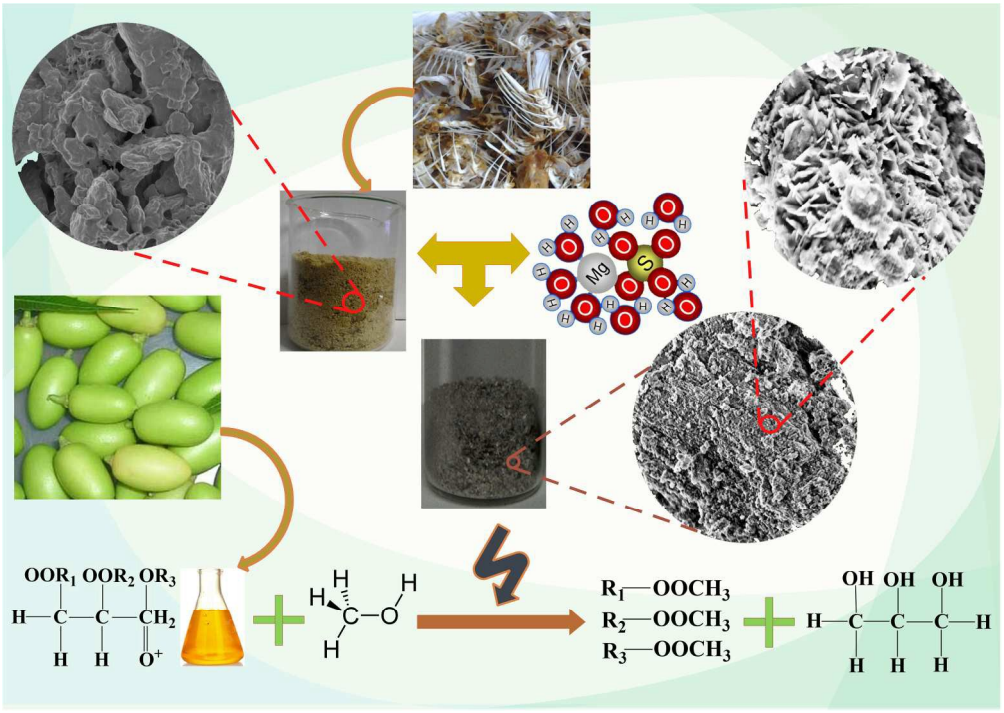

628x444mm (96 x 96 DPI)